ROBUST CONTROL DESIGN VIA STRUCTURED H-INFINITY FOR THE ATMOSPHERIC RE-ENTRY OF REUSABLE LAUNCHERS

Alice De Oliveira[(1)] **and Michèle Lavagna**[(1)]

[(1)]*Politecnico di Milano, Aerospace Science and Technology Department, Via Giuseppe La Masa 34, 20156 Milan, Italy, alice.deoliveira@polimi.it, michelle.lavagna@polimi.it*

ABSTRACT

This paper studies the synthesis of a robust control system via structured H_∞ for the full atmospheric re-entry problem of Reusable Launch Vehicles (RLVs). This control system is foreseen to be integrated in a nonlinear six-degree-of-freedom RLV re-entry dynamics simulator which covers the aerodynamic and powered descent phase until vertical landing of a first-stage rocket equipped with a thrust vector control system and steerable planar fins. The controllers are built at different points of the re-entry trajectory, using the H_∞ framework through PID-like structures with feedback on the attitude angles. The controller architecture is verified through linear analyses as well as nonlinear cases with the aforementioned simulator, and the control approach is validated by comparing the performance with a baseline controller. This study paves the way towards the design of a robust control system able to cope with the challenging RLV re-entry problem.

1 INTRODUCTION

Launcher reusability is now the new paradigm for a sustainable and cost-effective access to space. Whereas this technology was already developed in the Space Shuttle era, the shift took place less than ten years ago when the US private company SpaceX demonstrated the possibility to reuse commercial launch vehicles by landing the first stage of its Falcon 9 rocket after having put a payload in orbit, in December 2015 [1]. More particularly, in 2017, SpaceX's Falcon 9 was the first Vertical Take-Off Vertical Landing (VTVL) vehicle having its first stage recovered after launch and reused for another mission, and then became in 2020, the first private rocket to take astronauts to the International Space Station thanks to its cargo spacecraft Dragon [2]. Today, the company has flown reusable boosters more than 100 times, with some single boosters reused more than 10 times, therefore showing the success of such a technology. Consequently, other private companies such as Rocket Lab and Blue Origin are also developing competitive reusable rockets, while national space agencies and intergovernmental institutions are increasing the research and development on launcher reusability.
Reusable Launch Vehicle (RLV) atmospheric re-entry and precision soft-landing on Earth is very challenging as it depends on multiple parameters, further complicated by the dense terrestrial atmosphere [3]. It was made possible by the development of advanced and robust computational methods able to generate in real time the reference trajectory to be followed according to the flight conditions, and then to command the optimal vehicle's actuator deflections to steer the vehicle until the landing site. Despite the success of commercial space companies, some standing problems such as the aerodynamic and powered descent of the launcher, require further understanding. Indeed, during an Earth atmospheric re-entry, the vehicle is subjected to fast system dynamics changes partly induced by external loads associated with the terrestrial environment (e.g., lift, drag, wind and gusts),

but also by the actuation commands to answer the landing constraints satisfaction and the vehicle integrity preservation. All those involve uncertainties and nonlinearities, which lead to vehicle's instability and therefore justify the implementation of highly performant Guidance & Control (G&C) algorithms. More particularly, one of the critical aspects is the design of a robust control strategy capable of counteracting the previously defined disturbances and uncertainties while satisfying the strict accuracy requirements associated with the pinpoint landing. This synthesis is further complicated by the need for a real-time guidance algorithm updating onboard the optimal trajectory to be followed by the vehicle, and therefore which requires that the controller be capable of tracking multiple types of possible references.

As demonstrated by the current state-of-the-art on control design for launchers [4], [5], the classical linear control theory represents a rich heritage with a lot of applications. This choice was motivated by its relative easiness of implementation and the possibility to use gain-scheduling techniques to adapt to nonlinear systems. Nevertheless, these techniques are well-adapted to the control system design of Single-Input Single-Output (SISO) systems, such as for example a reusable rocket using a Thrust Vector Control (TVC) system as the unique actuator. The implementation of Multiple-Input Multiple-Output (MIMO) control systems becomes then complex since every channel is addressed in a single-loop fashion. This capability is however required for the future generation of reusable rocket, using also aerodynamic steering based on fins in addition to the TVC system for enhancing control authorities. Moreover, model uncertainties are not accurately considered in the design process, developed only with nominal conditions and stability margin requirements. For all these reasons, it results in an extensive (both in terms of time and cost) Verification and Validation campaign with many iterations and Monte-Carlo analyses to assess the performance and robustness of the control system.

To overcome these drawbacks, the H_∞ family of methods, introduced a few years ago [6], provides with a powerful solution for robust control design. It relies on defining the control requirements in the frequency domain in terms of weighting functions and minimizing the maximum gain of the resulting weighted system from the exogenous inputs to the outputs to be controlled. Moreover, the control-plant interaction is modelled through a Linear Fractional Transformation (LFT) representing the feedback action. Finally, the structured H_∞ method [7] allows to directly impose a specific control structure – like a Proportional-Integral-Derivative (PID), enabling the re-use of gain-scheduling techniques – and to consider parametric uncertainties for enhanced robustness. This technology was studied in the United States for the Ares-I, later Space Launch System program [8], and in Europe for Ariane 5 [9] and the future generation of European launchers [10]. Over the last years, several studies on this method for the atmospheric descent and landing phases of vehicles have emerged and show promising results. Whereas structured H_∞ was first mainly studied for the ascent phase of the VEGA launcher recovering the baseline control structure [11], some analyses were further achieved on the descent phase [12]. Robust control synthesis for descent and landing on small planetary bodies was also addressed with a robustness analysis via structured singular value to involve the parametric gravitational uncertainties directly in the control synthesis [13]. Moreover, interesting cases for the aerodynamic descent of reusable rockets were exploited on the framework of the CALLISTO project where first decoupled attitude and translational channels were considered for the design of robust controllers on each control axis [14], before considering an unified control for both position and attitude with a robustness analysis to account for uncertainties [15]. Finally, a multi-plant control design approach with fully-coupled translational and attitude dynamics was studied as a solution to better consider the range of trajectories coming from the online guidance algorithm during the flight [16].

It is clear from the available literature that this technology has been largely explored for the ascent phase of conventional (i.e. non reusable) launch vehicles and remains scarcely studied for the atmospheric re-entry of reusable rockets. Moreover, among most of the aforementioned literature, only

the aerodynamic descent phase using steerable planar fins was considered and the powered-descent phase combining fins and TVC was only treated in [12]. This paper investigates the problem of robust control design via structured H_∞ for the full atmospheric re-entry of RLVs, i.e. from the aerodynamic to the powered descent and landing, with a particular attention on coupling TVC system and steerable planar fins during the descent. Therefore the studied problem covers the atmospheric re-entry and vertical landing of a first-stage rocket equipped with both actuation systems. First, the nonlinear Six-Degree-of-Freedom (6-DoF) RLV re-entry are simplified into an efficient linear model decoupling the body axes' dynamics and then linearised along a reference trajectory to get the nominal LFT of the system, which can be augmented with parametric uncertainties. Second, the controllers are built at different points of the re-entry trajectory, using the structured H_∞ framework through PID-like structures. Weighting functions considering the control objectives as well as the stability and performance requirements of a realistic RLV re-entry scenario are implemented. Linear analyses are performed via classic stability margins to verify the control design. Finally, the controllers are gain-scheduled and validated via Monte-Carlo analyses, using a nonlinear 6-DoF RLV re-entry dynamics simulator equipped with successive convex optimisation guidance. The performance of the resulting closed-loop G&C system is compared with the baseline developed in previous works using a classical linear feedback control through gain-scheduled PID controllers [17].
The paper is organised as follows. Sec. 2 introduces the full-modelling of the nonlinear controlled dynamics involved in the atmospheric re-entry of reusable launchers, and more particularly the linearised model used for the control synthesis. Then, Sec. 3 formulates the robust control design via structured H_∞ with weighting functions adequately chosen according to the available requirements, and analyse the synthesised controllers with classic linear analysis techniques in Sec. 4. Subsequently, the nonlinear analysis coming from the use of the 6-DoF RLV re-entry dynamics simulator and the comparison with the previous baseline G&C system are performed in Sec. 5. Finally, conclusions and future works are provided in Sec. 6.

2 REUSABLE LAUNCHERS RE-ENTRY CONTROL PROBLEM

This section describes the nonlinear 6-DoF dynamics of a VTVL vehicle first-stage booster modelled as a rigid body with varying mass, subjected to external forces induced by the terrestrial atmosphere and controlled through embedded closed-loop guidance and control strategies. Therefore, the RLV re-entry dynamics simulator with its nonlinear equations of motion is described first, and then through its state-space realisation. Whereas the nonlinear simulator is used for the assessment of the synthesised controllers through time-domain analyses, the linear state-space representation is used for the control design through linearisation about an offline reference trajectory.

2.1 6-DoF nonlinear re-entry controlled dynamics

This paper relies on the 6-DoF reusable launchers re-entry controlled dynamics simulator developed by the authors to study the efficiency of aerodynamic steering and conventional G&C techniques [17]. Whereas in this previous research work, the vehicle was only steered via a TVC system and the fixed planar fins implementation was studied, the RLV simulator used in this paper considers a vehicle actuated both by the TVC system and steerable planar fins. An analysis to add an enhanced aerodynamic model in the simulator was carried out in [18] but the updated feature is not included in this study not to add complexity on the control design.
The simulator includes standard G&C algorithms where a thrust vector is commanded by the guidance subsystem and then converted to reference pitch $\theta_{ref}(t)$ and yaw $\psi_{ref}(t)$ angles, and thrust magnitude T_{ref}. Then, the control subsystem generates the necessary commands to correct the deviations between the reference and actual attitude angles in terms of TVC gimbal deflections $\{\beta_{TVC,y}, \beta_{TVC,z}\}$

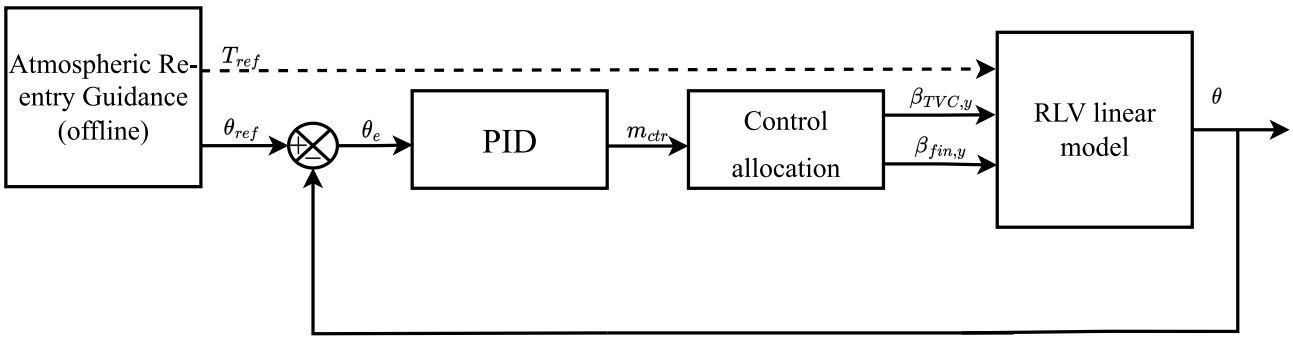

Figure 1: Structure for baseline control synthesis, adapted from [19].

and fins' deflections $\{\beta_{fin,y}, \beta_{fin,z}\}$. The guidance subsystem relies on a successive convex optimisation algorithm which consists in iteratively solving convex optimisation second order cone programming subproblems in which the non-convex dynamics and constraints are repeatedly linearised using the information coming from the previous iteration solution. The generated reference trajectory is updated with a frequency of $f_{gui} = 0.1$ Hz at which the guidance subsystem is re-executed in order to cope with the current flight conditions and improve accordingly the trajectory to be followed. Concerning the baseline control subsystem (i.e. before being replaced by the new structured H_∞ control synthesis), it relies on the use of feedback control though gain-scheduled PID controllers, decoupling pitch and yaw axes based on the assumption of low roll rates. To simplify the MIMO formulation due to the consideration of TVC and steerable planar fins, for which it is complex to apply classical linear control theory, a control moment is defined as a variable specifying the necessary pitch or yaw moment to be commanded to correct the trajectory of the vehicle, following the work in [19]. Then, knowing the control effectiveness level of each actuator, a control allocation algorithm is used to determine the actual control inputs in terms of TVC gimbal and fins' deflection angles. Fig. 1 illustrates this structure for the gain-scheduled PID controllers synthesis used as baseline, where a reference trajectory corresponding to the simulated case is stored offline and used through the RLV linear model to tune the scheduled PID controllers by sampling the system in n different points according to the altitude (the same template is used for H_∞ synthesis so more details are available in Sec. 3).
The equations of motion are written in the landing site-centered inertial and the vehicle's body-fixed reference frames. They are based on the initial state $\mathbf{x}_I(0) = \begin{bmatrix} m(0) & \mathbf{r}_I^T(0) & \mathbf{v}_I^T(0) & \mathbf{q}_B^I(0)^T & \boldsymbol{\omega}_B^T(0) \end{bmatrix}$ and on the assumptions that the vehicle is a rigid body with no effect induced by the varying mass (e.g. propellant sloshing) and structural flexibilities for the sake of simplicity. Therefore we can formulate the 6-DoF re-entry equations of motion of a powered RLV as described by the following set of nonlinear differential equations (1). Note that Eq. (1) implemented in the nonlinear simulator is therefore used for the validation of the control strategy in Sec. 5.

$$
\begin{aligned}
\dot{m}(t) &= -\frac{||\mathbf{F}_{TVC,I}(t)||_2}{I_{sp} g_0} - \frac{A_{nozzle} P_{amb}(t)}{I_{sp} g_0} \\
\dot{\mathbf{r}}_I(t) &= \mathbf{v}_I(t) \\
\dot{\mathbf{v}}_I(t) &= \frac{1}{m(t)} \left[\mathbf{F}_{TVC,I}(t) + \mathbf{F}_{fins,I}(t) + \mathbf{F}_{aero,I}(t) \right] + \mathbf{g}_I(t) \\
\dot{\mathbf{q}}_B^I(t) &= \frac{1}{2} \begin{bmatrix} q_4(t) & -q_3(t) & q_2(t) \\ q_3(t) & q_4(t) & -q_1(t) \\ -q_2(t) & q_1(t) & q_4(t) \\ -q_1(t) & -q_2(t) & -q_3(t) \end{bmatrix} \boldsymbol{\omega}_B(t) \\
\dot{\boldsymbol{\omega}}_B(t) &= J^{-1}(t) \left[\mathbf{M}_{TVC,B}(t) + \mathbf{M}_{fins,B}(t) + \mathbf{M}_{aero,B}(t) - \boldsymbol{\omega}_B(t) \times J \boldsymbol{\omega}_B \right]
\end{aligned}
\tag{1}
$$

In Eq. (1), $m(t)$ is the mass of the vehicle, $\mathbf{r}_I(t) \in \mathbb{R}^3$ and $\mathbf{v}_I(t) \in \mathbb{R}^3$ are the position and velocity at the center-of-gravity (CG) of the vehicle expressed in the inertial reference frame. The attitude states are governed by the quaternion-based kinematics equation where $\boldsymbol{\omega}_B(t) \in \mathbb{R}^3$ is the angular velocity vector expressed in the vehicle's body-fixed reference frame. I_{sp} is the vacuum specific impulse of the engine, g_0 is the standard Earth gravity, A_{nozzle} is the nozzle exit area of the engine, $P_{amb}(t)$ is the ambient atmospheric pressure and $J(t) = \text{diag}\left(\begin{bmatrix} J_A(t) & J_N(t) & J_N(t) \end{bmatrix}\right)$ is the inertia matrix of the vehicle. The terms $\mathbf{F}_{aero,I}(t) \in \mathbb{R}^3$ and $\mathbf{M}_{aero,B}(t) \in \mathbb{R}^3$ represent, respectively, the aerodynamic force and moment acting on the vehicle. The *spherical* aerodynamic model introduced by [20] is used and approximates the aerodynamic force as always anti-parallel with respect to the inertial velocity $\mathbf{v}_I(t)$, here without accounting for wind. Therefore, assuming that the rocket is axisymmetric, the aerodynamic force and moment are expressed by:

$$\begin{aligned} \mathbf{F}_{aero,B}(t) &= -\frac{1}{2}\rho(t) V S_{ref} C_{aero} \mathbf{v}_B(t) \\ \mathbf{F}_{aero,I}(t) &= \mathbf{R}_I^B(t) \mathbf{F}_{aero,B}(t) \\ \mathbf{M}_{aero,B}(t) &= [\mathbf{x}_{CP} - \mathbf{x}_{CG}(t)] \times \mathbf{F}_{aero,B}(t) \end{aligned} \tag{2}$$

where $V = ||\mathbf{v}_I(t)||_2$ is the norm of the velocity vector, $\mathbf{R}_B^I(t)$ represents the rotation matrix from the inertial reference frame to the vehicle's body-fixed reference frame, S_{ref} is the reference aerodynamic area of the vehicle, and $\mathbf{x}_{CP} = \begin{bmatrix} x_{CP} & 0 & 0 \end{bmatrix}^T$ and $\mathbf{x}_{CG} = \begin{bmatrix} x_{CG}(t) & 0 & 0 \end{bmatrix}^T$ represent, respectively, the center of pressure (CP) and the CG. C_{aero} is the aerodynamic coefficient matrix defined by $C_{aero} = \text{diag}\left(\begin{bmatrix} c_{a,x} & c_{a,x} & c_{a,x} \end{bmatrix}\right)$ where $c_{a,x}$ is a positive scalar considered assumed constant during all the flight. Then, the gravitational field is defined in the inertial frame as a function of the altitude $r_{I,x}(t)$:

$$\begin{aligned} \mathbf{g}_I(r_{I,x}(t)) &= \begin{bmatrix} g(r_{I,x}(t)) & 0 & 0 \end{bmatrix}^T \\ g(r_{I,x}(t)) &= g_0 \left(\frac{R_E}{R_E + r_{I,x}(t)} \right)^2 \end{aligned} \tag{3}$$

where R_E is the radius of the Earth. Finally, the terms $\mathbf{F}_{TVC,I}(t) \in \mathbb{R}^3$, $\mathbf{M}_{TVC,B}(t) \in \mathbb{R}^3$ and $\mathbf{F}_{fins,I}(t) \in \mathbb{R}^3$, $\mathbf{M}_{fins,B}(t) \in \mathbb{R}^3$ correspond respectively to the forces and moments acting on the vehicle coming from the TVC system and the steerable planar fins. The TVC system actuates by deflecting the engine's nozzle by $\beta_{TVC,y}(t)$ and $\beta_{TVC,z}(t)$, respectively along the body pitch and yaw axes. It is modelled with the thrust magnitude $T_{ref}(t)$ directly coming from the guidance algorithm to enable the decoupling between translational and rotational dynamics. Therefore the TVC-generated force and moment can be expressed by:

$$\begin{aligned} \mathbf{F}_{TVC,B}(t) &= T_{ref}(t) \begin{bmatrix} \cos\left(\beta_{TVC,y}(t)\right) \cos\left(\beta_{TVC,z}(t)\right) \\ \cos\left(\beta_{TVC,y}(t)\right) \sin\left(\beta_{TVC,z}(t)\right) \\ -\sin\left(\beta_{TVC,y}(t)\right) \end{bmatrix} \\ \mathbf{F}_{TVC,I}(t) &= \mathbf{R}_I^B(t) \mathbf{F}_{TVC,B}(t) \\ \mathbf{M}_{TVC,B}(t) &= [\mathbf{x}_{PVP} - \mathbf{x}_{CG}(t)] \times \mathbf{F}_{TVC,B}(t) \end{aligned} \tag{4}$$

with $\mathbf{x}_{PVP} = \begin{bmatrix} x_{PVP} & 0 & 0 \end{bmatrix}^T$ the TVC pivot position. Following the planar fins model of [17] adapted from [19], the steerable fins model applied in this study is considering two pairs of fins placed above the vehicle's CG: one pair, with deflections $\beta_{fin,1}(t) = \beta_{fin,2}(t) = \beta_{fin,y}(t)$, is controlling the motion in the pitch plane while the other, with $\beta_{fin,3}(t) = \beta_{fin,4}(t) = \beta_{fin,z}(t)$, is controlling the motion in the yaw plane. It is further assumed that, due to the reduced fin area compared to the RLV body, only the normal force contribution is considered and the normal coefficient of the fin is estimated using lifting-line theory for a symmetric airfoil [21] by $C_{N,fin}(\gamma_{fin,i}(t)) = 2\pi \left(\frac{AR_{fin}}{AR_{fin}+2} \right) \sin\left(\gamma_{fin,i}(t)\right)$,

where $\gamma_{fin,i}(t)$ is the i-th fin local angle of attack and AR_{fin} is the aspect ratio of the fin. Based on these assumptions, the fins' force and moment contributions in the pitch plane are expressed in the vehicle's body-fixed reference frame by:

$$\begin{aligned}
\gamma_{fin,i}(t) &= \beta_{fin,i}(t) - \alpha(t) \\
\mathbf{F}_{fin,i}(t) &= \frac{1}{2}\rho(t)V^2 S_{fin} C_{N,fin}(\gamma_{fin,i}(t)) \begin{bmatrix} -\sin(\beta_{fin,i}(t)) & 0 & \cos(\beta_{fin,i}(t)) \end{bmatrix}^T, \quad i = \{1,2\} \\
\mathbf{M}_{fin,i}(t) &= [\mathbf{x}_{fin,i} - \mathbf{x}_{CG}(t)] \times \mathbf{F}_{fin,i}(t)
\end{aligned} \tag{5}$$

where $\alpha(t)$ is the vehicle's angle of attack, S_{fin} is the fin reference area and $\mathbf{x}_{fin,i} = \begin{bmatrix} x_{fin,i} & 0 & 0 \end{bmatrix}^T$ is the longitudinal i-th fin position. And similarly, the following contributions are obtained in the yaw plane:

$$\begin{aligned}
\gamma_{fin,i}(t) &= -\beta_{fin,i}(t) - \beta(t) \\
\mathbf{F}_{fin,i}(t) &= \frac{1}{2}\rho(t)V^2 S_{fin} C_{N,fin}(\gamma_{fin,i}(t)) \begin{bmatrix} \sin(\beta_{fin,i}(t)) & \cos(\beta_{fin,i}(t)) & 0 \end{bmatrix}^T, \quad i = \{3,4\} \\
\mathbf{M}_{fin,i}(t) &= [\mathbf{x}_{fin,i} - \mathbf{x}_{CG}(t)] \times \mathbf{F}_{fin,i}(t)
\end{aligned} \tag{6}$$

where $\beta(t)$ is the vehicle's sideslip angle. Finally, the total force generated by the steerable planar fins in the inertial reference frame and the total moment generated in the vehicle's body-fixed reference frame are given by:

$$\begin{aligned}
\mathbf{F}_{fins,I}(t) &= \mathbf{R}_I^B(t) \sum_{i=1}^{4} \mathbf{F}_{fin,i}(t) \\
\mathbf{M}_{fins,B}(t) &= \sum_{i=1}^{4} \mathbf{M}_{fin,i}(t)
\end{aligned} \tag{7}$$

Since the relationships in Eqs. (1-7) are nonlinear, it is therefore needed to formulate the system through a state-space representation compatible for H_∞ synthesis.

2.2 State-space representation

Before proceeding with the linearisation of the equations of motion depicted in Eq. 1, several assumptions must be made. First, the launch vehicle is considered axisymmetric with a negligible roll rate, therefore allowing the decoupling of the motion in the pitch and yaw planes. The wind disturbances are not considered at this stage, knowing that this feature could be added in future work following the scheme available in literature [12], [15]. Finally, the effects of actuators, bending and sloshing dynamics are ignored for the sake of simplicity. In this subsection, only the pitch dynamics will be defined for conciseness but the expressions obtained for the yaw dynamics are similar. Fig. 2 displayed the rocket descent dynamics in the pitch plane.
The pitch dynamics are therefore described with the following state-space equations obtained by the linearisation of the perturbed equations of motion (1) translated in the vehicle's body fixed reference frame. Note that the Δ symbol referring to the perturbed variables is here omitted but that we clearly refer to the variations with respect to their reference value.

$$\begin{bmatrix} \dot{\theta} & \ddot{\theta} & \dot{z}_B & \ddot{z}_B \end{bmatrix}^T = A_{RLV} \begin{bmatrix} \theta & \dot{\theta} & z_B & \dot{z}_B \end{bmatrix}^T + B_{RLV} \begin{bmatrix} \beta_{TVC,y} & \beta_{fin,y} \end{bmatrix}^T \tag{8}$$

where θ, $\dot{\theta}$ and $\ddot{\theta}$ represent pitch angle and first/second-order derivatives and z_B, $\dot{z_B}$ and $\ddot{z_B}$ are the

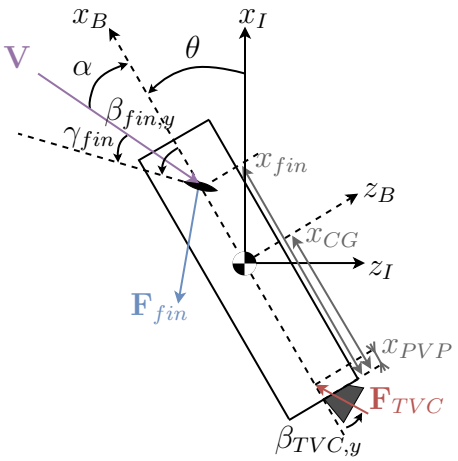

Figure 2: Rocket descent pitch dynamics

lateral drift and derivatives. The matrices A_{RLV} and B_{RLV} are defined by:

$$A_{RLV} = \begin{bmatrix} 0 & 1 & 0 & 0 \\ 0 & 0 & 0 & \mu_{LV} + \frac{\mu_{fin,\gamma}\cos(\beta_{fin,y0})}{V\cos(\alpha_0)} \\ 0 & 0 & 0 & 1 \\ -a_0 & u_0 & 0 & -\left(N_{LV} + \frac{N_{fin,\gamma}\cos(\beta_{fin,y0})}{mV\cos(\alpha_0)}\right) \end{bmatrix}$$
$$B_{RLV} = \begin{bmatrix} 0 & 0 \\ -\mu_{TVC}\cos(\beta_{TVC,y0}) & -\mu_{fin,\gamma}\cos(\beta_{fin,y0}) \\ 0 & 0 \\ -\frac{T}{m}\cos(\beta_{TVC,y0}) & \frac{N_{fin,\gamma}}{m}\cos(\beta_{fin,y0}) \end{bmatrix} \tag{9}$$

where the aerodynamic, fin and TVC moment and force coefficients are given by:

$$N_{LV} = \frac{1}{2}\rho V S_{ref} c_{a,x}, \quad N_{fin,\gamma} = \rho V^2 S_{fin} C_{N,fin\backslash\gamma}$$
$$\mu_{LV} = \frac{N_{LV}}{J_N} l_\gamma, \quad \mu_{fin,\gamma} = \frac{N_{fin,\gamma}}{J_N} l_{fin}, \quad \mu_{TVC} = \frac{T_{ref}}{J_N} l_{TVC} \tag{10}$$

where $C_{N,fin\backslash\gamma} = 2\pi\left(\frac{AR_{fin}}{AR_{fin}+2}\right)\cos(\gamma_{fin,y0})$ is the fin normal force gradient and with $l_\gamma = x_{CP} - x_{CG}$, $l_{fin} = x_{fin} - x_{CG}$ and $l_{TVC} = x_{CG} - x_{PVP}$. The trim velocity and acceleration are defined by:

$$u_0 = V\cos(\alpha_0), \quad a_0 = g\cos(\theta_0)\cos(\psi_0) \tag{11}$$

Therefore, the state-space representation of Eq. (8) and the corresponding one for yaw dynamics have been used for the control synthesis developed in the next section.

3 ROBUST CONTROL DESIGN VIA STRUCTURED H_∞ SYNTHESIS

In this section, gain-scheduled structured H_∞ controllers are designed for the aerodynamic and powered descent phase of an RLV along a reference trajectory computed offline, using the state-space representation developed in the previous section. This control technique has indeed been demonstrated as a successful candidate in space applications to cope with the closed-loop requirements needed to enable robustness and performance [11], [15], [16]. More particularly in this study, the requirements include closed-loop stability and attitude tracking (pitch and yaw angle errors must be

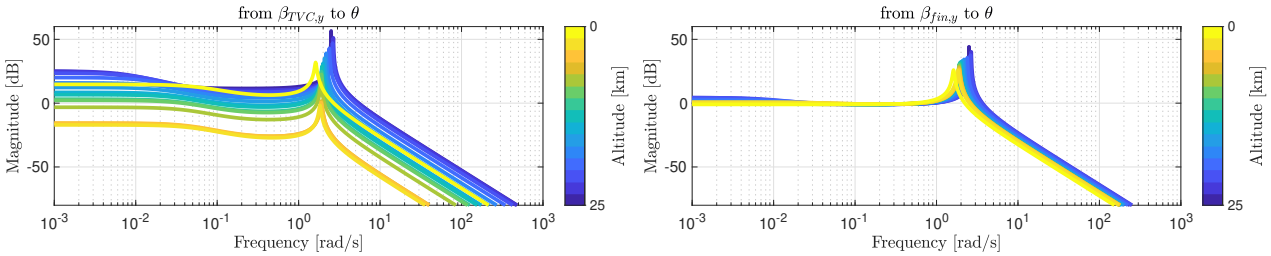

(a) From TVC to pitch angle

(b) From fins to pitch angle

Figure 3: System transfer function with respect to altitude.

less than 5 deg), and actuation limitation ($\beta_{TVC,i} \leq 10$ deg, $\beta_{fin,i} \leq 20$ deg). More requirements regarding position and velocity, and disturbance rejection (e.g. wind) are not considered since the first objective of this work is to recover the baseline control system including gain-scheduling PID controllers described in Fig. 1 of the previous section.

3.1 Control architecture

The system constituted by the RLV linear dynamics model developed previously is subjected to significant changes through the descent flight, mainly due to the variations associated to the thrust and aerodynamics. Indeed, Fig. 3 shows the Bode plot of the actuators (TVC and fins) to pitch angle channel where the linear dynamics are discretised according to the altitude with $n = 15$ points. Therefore, it justifies the use of gain-scheduling to increase the performance and robustness of the control system. The altitude has been chosen as the scheduling parameter since it is monotonically evolving with respect to time and has been well validated in the literature [15], [16]. The 15 points were equally distributed with respect to the altitude vector which allows to well capture the variations in terms of thrust magnitude and dynamic pressure.

In the framework of structured H_∞, the augmented plant must be defined. It is usually constituted of the linear dynamics model of the system, the controller to be designed, other linear systems describing the effects of the actuators (TVC and fins) or disturbances such as wind, and a set of weights which include design specifications. Note that in this study, for the sake of simplicity, the effect of sensors, actuators and wind disturbances are not considered. In order to recover the previously designed control structure explained in Sec. 2, a PID structure is used for the controllers to be designed, taking the pitch angle error θ_e as input and giving the actuator deflections $\{\beta_{TVC,y}, \beta_{fin,y}\}$ as outputs. Note that here the synthesis is depicted for the pitch dynamics but the same methodology is followed for the yaw dynamics. Fig. 4 shows the augmented plant named $P(s)$.

The exogenous input is the reference pitch angle θ_{ref}, scaled by the constant input weighting function W_c, which translates it into the signal θ_c. The comparison of the scaled reference θ_c and the output pitch angle θ generates the pitch angle error θ_e entering the controller $K^\theta(s) = \begin{bmatrix} K^\theta_{TVC}(s) & K^\theta_{fin}(s) \end{bmatrix}^T$. Then the deflection angles $\{\beta_{TVC,y}, \beta_{fin,y}\}$ enter the RLV linear dynamics model. The mixed $T/S/KS$ sensitivity approach is employed for design tuning where the output weighting functions W_t, W_e, and $W_u = \text{blkdiag}\begin{bmatrix} W_{u,TVC} & W_{u,fin} \end{bmatrix}$ shape the tracking performance, the disturbance rejection capability and the control efforts, respectively. More particularly, the controller is defined by:

$$K^\theta(s) = \begin{bmatrix} K^\theta_{TVC}(s) \\ K^\theta_{fin}(s) \end{bmatrix}, \quad K^\theta_{TVC}(s) = \left(K_{p,TVC} + \frac{K_{i,TVC}}{s} + \frac{K_{d,TVC}s}{1 + T_{f,TVC}s} \right) \theta_e, \quad K^\theta_{fin}(s) = \left(K_{p,fin} + \frac{K_{i,fin}}{s} + \frac{K_{d,fin}s}{1 + T_{f,fin}s} \right) \theta_e \tag{12}$$

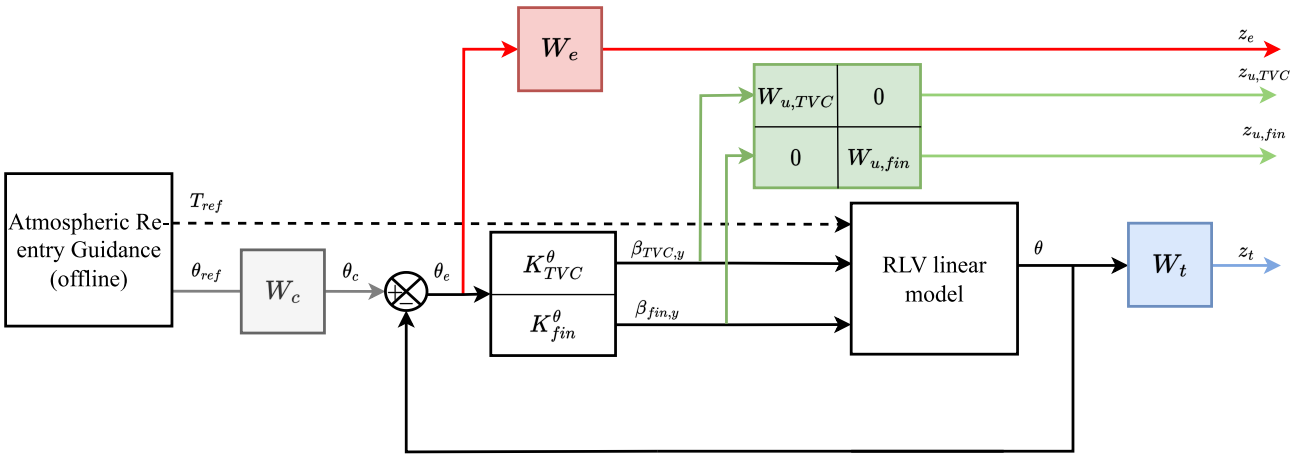

Figure 4: Pitch control augmented plant $P(s)$.

Therefore, the objective of the H_∞ optimal control problem is to find the gains $K_{p,TVC}$, $K_{i,TVC}$, $K_{d,TVC}$, $T_{f,TVC}$ and $K_{p,fin}$, $K_{i,fin}$, $K_{d,fin}$, $T_{f,fin}$ which constitute a stabilising controller K^θ such that the H_∞-norm of the augmented system is minimised. The optimal problem is defined by:

$$\min_{K^\theta} ||P_{\theta_{ref}\to\mathbf{z}}(s)||_\infty \tag{13}$$

where $\mathbf{z} = \begin{bmatrix} z_e & z_t & \mathbf{z}_u \end{bmatrix}^T$, with $\mathbf{z}_u = \begin{bmatrix} z_{u,TVC} & z_{u,fin} \end{bmatrix}^T$. Eq. (13) leads to a non-smooth, non-convex optimisation problem which can be solved with available tools [7], particularly implemented in the Robust Control Toolbox of MATLAB, *hinfstruct* or *systune*. The former was used in this study.

3.2 Weighting functions selection

The definition of the weighting functions is substantial to obtain good performance and robustness as mentioned before. The input weighting function W_c used for reference scaling is determined based on the allowed maximum value for the input reference, here the pitch angle. For this study, we set:

$$W_c(s) = \frac{\pi}{180} \text{ rad} \tag{14}$$

The output weighting functions W_t, W_e and W_u must complete the $T/S/KS$ mixed sensitivity synthesis problem. Indeed, their inverse bound respectively the complementary sensitivity function T, the sensitivity function S and the control sensitivity function KS. Usually W_e^{-1} is chosen as a high-pass filter whereas W_t^{-1} and W_u^{-1} are chosen as low-pass filters [11]. Therefore, the pitch angle error weighting function is defined as follows:

$$W_e^{-1}(s) = \frac{\pi}{180} \frac{h_e s + \omega_e}{s + \frac{\omega_e}{l_e}} \tag{15}$$

where the low-frequency $l_e = 0.001$ is chosen small to reduce the steady-state tracking error and $h_e = 1.5$ to keep small the maximum peak of the sensitivity function, which is critical to ensure good stability margins. ω_e is the desired bandwidth set as $\omega_e \in [0.45, 2.5]$ rad/s according to the design point studied. Then, W_t^{-1} is selected as:

$$W_t^{-1}(s) = \frac{\pi}{180} \frac{h_t s + \omega_t}{s + \frac{\omega_t}{l_t}} \tag{16}$$

where $l_t = h_e$ to keep the fundamental relationship between complementary sensitivity and sensitivity functions and reduce the parameters to be tuned, while $h_t = 0.001$. The tracking bandwidth is set to $\omega_t = 10$ rad/s. Finally, the control input weight matrix is here used to impose signal limitations in order to prevent from actuator saturation. They are set using constant weighting functions as followed:

$$\begin{aligned} W_u^{-1}(s) &= \text{blkdiag}\left[W_{u,TVC}^{-1}(s) \quad W_{u,fin}^{-1}(s)\right], \\ W_{u,TVC}^{-1}(s) = \frac{\pi}{180}5 \text{ rad}, &\quad W_{u,fin}^{-1}(s) = \frac{\pi}{180}2.5 \text{ rad} \end{aligned} \tag{17}$$

Note that the values of the control weighting functions have been selected lower than the maximum actuator deflections considered in the simulator ($\beta_{TVC,max} = 10$ deg, $\beta_{fin,max} = 20$ deg) to ensure that the actuators are not saturated during the descent flight.

4 LINEAR ANALYSIS

This section shows the linear analysis results obtained applying the structured H_∞ synthesis explained in Sec. 3. This analysis is necessary to validate the obtained controllers according to the requirements set previously but also according to the stability margins. For this study, following the work of [11], we expect a gain margin superior to 6 dB and a phase margin superior to 30 deg.
First, the frequency-domain results are analysed looking at the sensitivity, complementary sensitivity and control sensitivity functions. The corresponding plots are depicted in Fig. 5. The performance is quite good overall, the complementary sensitivity function (Fig. 5b) and the sensitivity function (Fig. 5a) do not show peaks which is a good indicator for stability margins. Note that the sensitivity functions for all the controllers are well below the corresponding weighting functions W_e^{-1} which validates the disturbance rejection requirement, but they are not represented since they vary according to the design point studied. Concerning the control sensitivity functions, depicted in Fig. 5c for the TVC system, and in Fig. 5d for the steerable planar fins, the requirements are also well met since the functions are below the weighting functions $W_{u,TVC}^{-1}$ and $W_{u,fin}^{-1}$. However, for some design points we can observe a peak at the same frequency than those observed in the transfer functions of the system (recall Fig. 3). The controllers are therefore generating an inverse peak to compensate for the

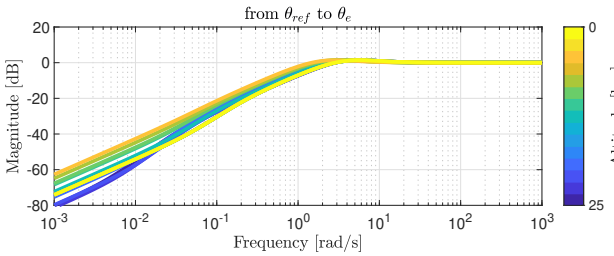

(a) Sensitivity function S

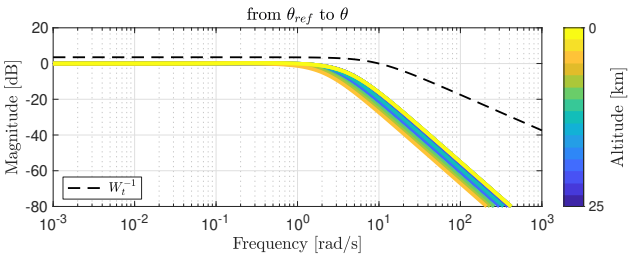

(b) Complementary sensitivity function T

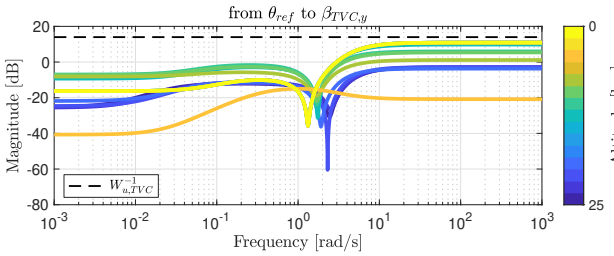

(c) TVC control sensitivity function $K_{TVC}^{\theta}S$

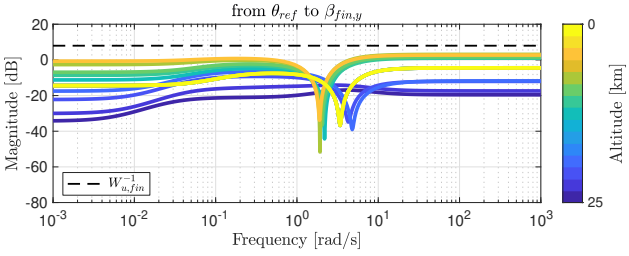

(d) Fin control sensitivity function $K_{fin}^{\theta}S$

Figure 5: Frequency-domain linear analyses of the controllers.

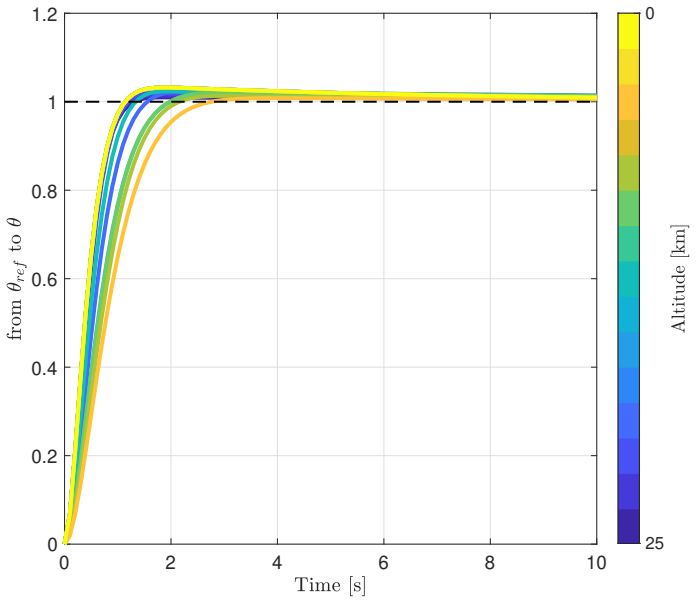

Figure 6: Step response for the controllers.

one existing in the system. Even if these controllers well enable to control the system in nominal conditions, they could not ensure sufficient stability margins in case of uncertainties in the system. This will particularly be analysed in Sec. 5.
Then, the time domain is also analysed by plotting the step response in Fig. 6. From this plot we can observe good tracking capabilities without a significant overshoot and with a relatively fast response. It is possible to see that the response is faster at the beginning and relatively slower towards the end. This is due to the high dynamic pressure at the beginning of the descent flight allowing more control authorities from the steerable planar fins. At low altitudes we actually notice that the response is faster again, more likely due to the high thrust magnitude increasing the control authority of the TVC system.

5 NONLINEAR SIMULATIONS

Once the design is satisfactory from the point of view of linear analysis, the next step is to implement the gain-scheduled controllers in the 6-DoF closed-loop RLV simulator described in Sec. 2 in order to assess them through nonlinear simulations. In this first subsection (Sec. 5.1), nonlinear simulations are carried out for the nominal conditions and compared with the baseline controller. In the second (Sec. 5.2), Monte-Carlo analyses are achieved to study the robustness of the controller to disturbances and uncertainties.

5.1 Nominal conditions

The gain-scheduled controllers synthesised with structured H_∞ are therefore implemented in the 6-DoF nonlinear re-entry dynamics simulator in closed-loop with the guidance algorithm and the flight mechanics involved. Since the idea of this work is to achieve a preliminary study of the robust structured H_∞ synthesis and recover the baseline control structure developed in previous works, the aerodynamic model considered in the nominal simulation is highly simplified with a pure drag force with constant drag coefficient ($c_{a,x} = 0.82$) and no wind is implemented during the descent. Moreover, only rigid-body motion is applied and propellant sloshing dynamics as well as structural flexibilities are ignored. The initial and final conditions of the nominal case are summarised in Tab. 1.

Table 1: Initial and final conditions

(a) Initial conditions

Parameter	Value
$\mathbf{r}_I[0]$	$[25,000 \quad 0 \quad -15,000]^T$ m
$\mathbf{v}_I[0]$	$[-850 \quad -0.1 \quad 950]^T$ m/s
$\boldsymbol{\omega}_B[0]$	$[0 \ 0 \ 0]^T$ rad/s
$m[0]$	14,000 kg

(b) Final conditions

Parameter	Value
$\mathbf{r}_I[K]$	$[0 \ 0 \ 0]^T$ m
$\mathbf{v}_I[K]$	$[-5 \ 0 \ 0]^T$ m/s
$\boldsymbol{\omega}_B[K]$	$[0 \ 0 \ 0]^T$ rad/s
$\mathbf{q}_B^I[K]$	$[0 \ 0 \ 0 \ 1]^T$

Fig. 7 compares the nominal trajectories in the pitch plane obtained for both control design, the baseline control in Fig. 7a and the structured H_∞ synthesis in Fig. 7b. The corresponding actuators' deflections and the pitch angle error throughout the descent flight are displayed. Both simulations have similar performance results in terms of final mass, final downrange error and final velocity error. It is possible to notice that the TVC deflection angle profiles are relatively similar at the beginning of the descent. Note that for the baseline control structure case, from around 40 s the TVC system is not actuated anymore due to the control allocation strategy used (recall Sec. 2), meaning that the steerable planar fins have more control authority at this stage of the descent and are not saturated. The fins deflection angle profiles are different and more particularly the sign of the deflection angle is reversed from 40 to 80 s. However, this is more likely due to a change of sign of the angle of attack at 40 s for the nonlinear simulation with the baseline control structure. Concerning the pitch angle error profiles, they are both inside the desired bounds, however, slight oscillations can be seen for the structured H_∞ design which is indicating a lack of stability of the controllers and also explaining why the deflections angles are higher in the second part of the trajectory compared to the baseline control structure case where the pitch angle error is close to 0 deg. From this comparison, the structured H_∞ synthesis for the controllers developed in this study is validated and satisfactory since it was possible to recover similar performance results. Nevertheless, the controllers should ensure a greater stability, also to enable a greater robustness towards uncertainties which is the topic of the next subsection. Future work will consider a new tuning of the controllers to get better performance and stability.

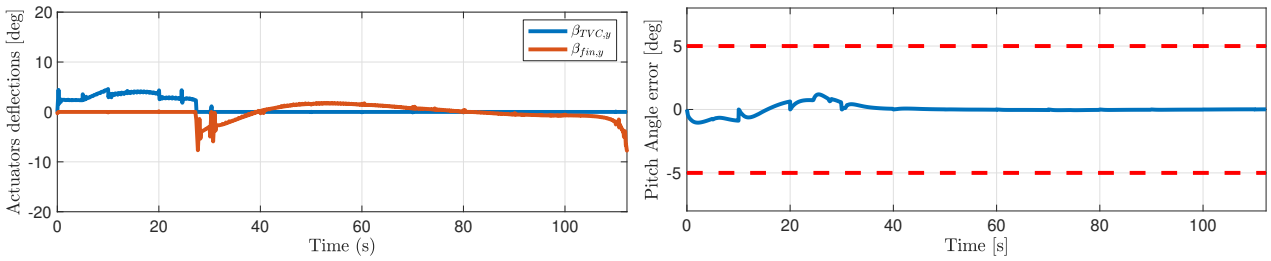

(a) Baseline control structure

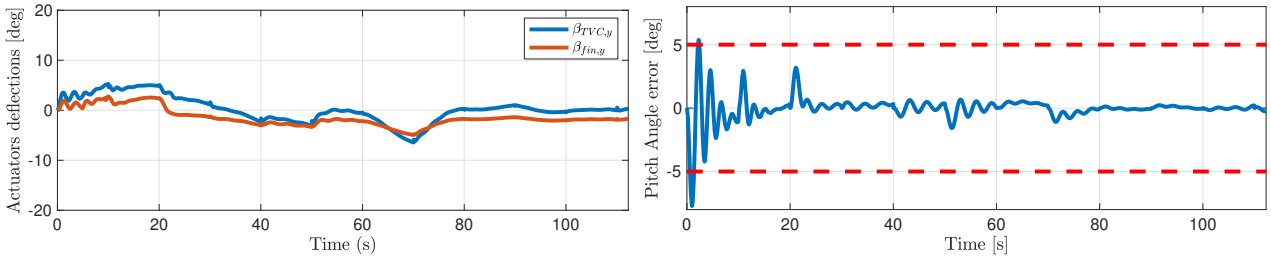

(b) Structured H_∞ control structure

Figure 7: Comparison of the baseline and H_∞ control structure for the nominal nonlinear simulation case.

5.2 Monte-Carlo analyses

The next step is to verify that the designed control system is able to be efficient even in the presence of multiple uncertainties and disturbances. Therefore, a 100-run Monte-Carlo analysis has been carried out for both control systems adding dispersions in critical parameters. More particularly, a normal distribution was considered for the lateral velocity $v_{I,z}$ with a standard deviation of 20 m/s. Then, uniform distributions of 5% were considered for the initial mass m_0 and the moments of inertia $J_A(t)$ and $J_N(t)$, whereas 10% were considered for the atmospheric density $\rho(t)$ and the ambient pressure $P_{amb}(t)$, and 20% for the drag coefficient $c_{a,x}$. The results in terms of actuators' deflection angles and pitch angle error as function of the altitude are depicted in Fig. 8.
Among the simulations carried out, 60% have been successful for the baseline control structure whereas only 8% for the structured H_∞ control. The failures are due to convergence issues of the guidance algorithm which did not always manage to find an optimal trajectory to be followed. Since these cases ended up before reaching the landing site, they do not provide any interesting information and therefore they are not represented in Fig. 8. From the available results, it is therefore possible to conclude that the controllers synthesised with the structured H_∞ method are not robust enough towards uncertainties and disturbances and therefore deserve a re-tuning with enhanced stability and robustness to uncertainties.

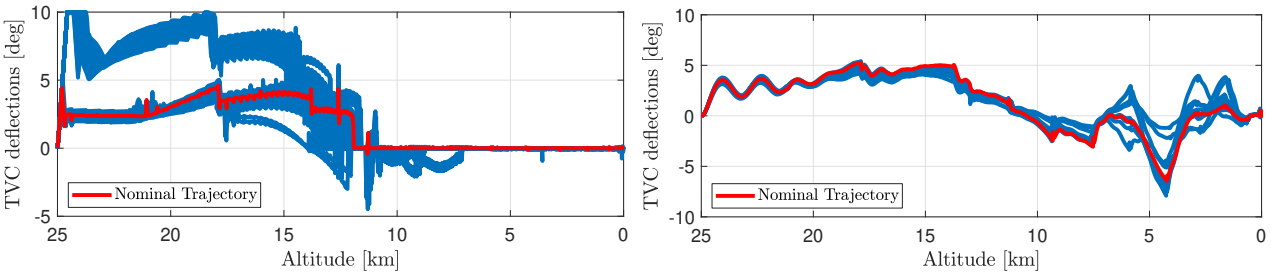

(a) TVC deflection angles

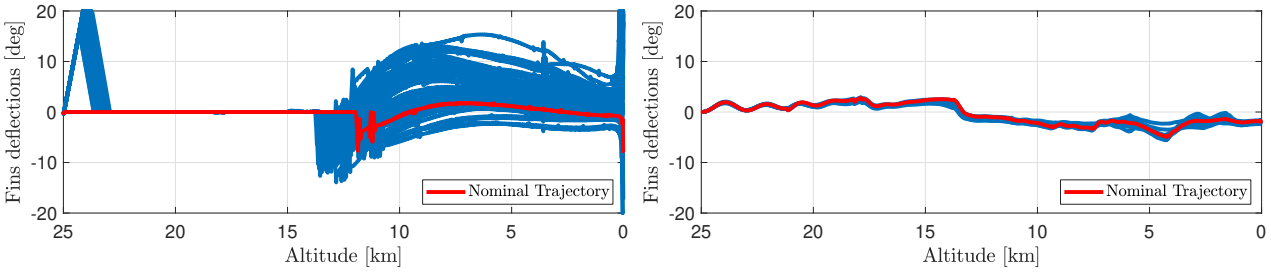

(b) Fins' deflection angles

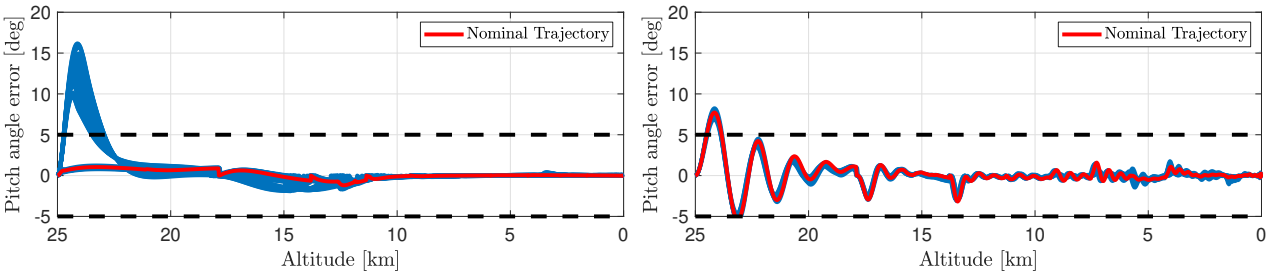

(c) Pitch angle error

Figure 8: Monte-Carlo analyses for the baseline (left column) and H_∞ control structure (right column) for the nominal nonlinear simulation case. The nominal trajectories obtained before are represented in red. Note that only the successful cases are plotted (60% for the baseline, only 8% for the H_∞).

6 CONCLUSIONS

In this paper, the implementation of structured H_∞ gain-scheduled controllers for the full aerodynamic and powered descent phase of reusable launchers was studied. This advanced control technique has been used to design controllers able to generate in one unified loop the necessary inputs to be commanded by the available actuators, TVC and steerable planar fins. Moreover, it enables the consideration of performance and stability requirements and control effort limitations, as well as an interesting versatility in terms of the control structure used with the possible integration of disturbances in the design for enhanced performance towards uncertainties. In this study, the objective was to recover the baseline control architecture used in previous works with gain-scheduled PID controllers on the attitude angle errors synthesised from classic linear control theory. Linear analysis in both time and frequency domain, and nonlinear analyses with a 6-DoF RLV re-entry dynamics simulator validate the control approach but also highlight the need for more stability and robustness towards uncertainties.
In this direction, further developments will perform a re-tuning of the controllers' gains with tighter stability margins and include a robustness analysis via μ-analysis considering directly uncertainties in the linear RLV model. Finally, although preliminary, this study shows the large capabilities of structured H_∞ synthesis to design a robust control system for high-demanding scenarios such as the aerodynamic and powered descent of reusable launchers which requires the coupling between steerable planar fins and TVC system as actuators.

7 ACKNOWLEDGEMENTS

The author would like to acknowledge and give thanks for the support and help of Pietro Ghignoni to develop the structured robust control during a 6-month visiting period at Deimos Space S.L.U. in Madrid, Spain. The project leading to this application has received funding from the European Union's Horizon 2020 research and innovation programme under the Marie Skłodowska-Curie grant agreement No 860956.

REFERENCES

[1] M. Wall. "Wow! SpaceX lands orbital rocket successfully in historic first," Space.com. (2015), [Online]. Available: https://www.space.com/31420-spacex-rocket-landing-success.html (visited on 05/18/2023).

[2] E. Howell. "SpaceX: Facts about Elon Musk's private spaceflight company," Space.com. (2022), [Online]. Available: https://www.space.com/18853-spacex.html (visited on 05/18/2023).

[3] L. Blackmore, "Autonomous precision landing of space rockets," *The Bridge on Frontiers of Engineering*, vol. 4, no. 46, pp. 15–20, 2016.

[4] C. Roux and I. Cruciani, "Scheduling schemes and control law robustness in atmospheric flight of VEGA," Proceedings of the 7th International ESA Conference on Guidance, Navigation and Control Systems, Tralee, County Kerry, Ireland 2-5 June 2008, 2008.

[5] E. Mooij, *Linear quadratic regulator design for an unpowered, winged re-entry vehicle* (08 Astrodynamics and Satellite Systems 03). Delft University Press, 1998, ISBN: 9040715971.

[6] J. Doyle, K. Glover, P. Khargonekar, and B. Francis, "State-space solutions to standard H2 and H∞ control problems," *IEEE Transactions on Automatic Control*, vol. 34, no. 8, pp. 831–847, 1989. DOI: 10.1109/9.29425.

[7] P. Apkarian and D. Noll, "Nonsmooth H∞ synthesis," *IEEE Transactions on Automatic Control*, vol. 51, no. 1, pp. 71–86, Jan. 2006. DOI: 10.1109/tac.2005.860290.

[8] W. Du, "Dynamic modeling and ascent flight control of Ares-I Crew Launch Vehicle," Ph.D. dissertation, Iowa State University, 2010.

[9] D. Saussie, Q. Barbes, and C. Berard, "Self-scheduled and structured H-infinity synthesis : A launch vehicle application," in *2013 American Control Conference*, IEEE, Jun. 2013. DOI: 10.1109/acc.2013.6580062.

[10] M. Ganet-Schoeller, J. Desmariaux, and C. Combier, "Structured control for future european launchers," *AerospaceLab Journal*, vol. Issue 13, December 2017, ISSN: 2107–6596, 2017. DOI: 10.12762/2017.AL13-08.

[11] D. Navarro-Tapia, A. Marcos, P. Simplicio, S. Bennani, and C. Roux, "Legacy recovery and robust augmentation structured design for the VEGA launcher," *International Journal of Robust and Nonlinear Control*, vol. 29, no. 11, pp. 3363–3388, Apr. 2019. DOI: 10.1002/rnc.4557.

[12] P. Simplicio, A. Marcos, and S. Bennani, "New control functionalities for launcher load relief in ascent and descent flight," Proceedings of the 8th European Conference for Aeronautics and Space Sciences. Madrid, Spain, 1-4 july 2019, 2019. DOI: 10.13009/EUCASS2019-275.

[13] P. Simplicio, A. Marcos, E. Joffre, M. Zamaro, and N. Silva, "Synthesis and analysis of robust control compensators for space descent and landing," *International Journal of Robust and Nonlinear Control*, vol. 28, no. 13, pp. 3871–3892, May 2018. DOI: 10.1002/rnc.4109.

[14] M. Sagliano, T. Tsukamoto, A. Heidecker, *et al.*, "Robust control for reusable rockets via structured H-infinity synthesis," Proceedings of the 11th International ESA Conference on Guidance, Navigation & Control Systems. Virtual Event, 22-25 June 2021, 2021.

[15] M. Sagliano, J. A. M. Hernández, S. Fari, *et al.*, "Unified-loop structured H-infinity control for aerodynamic steering of reusable rockets," *Journal of Guidance, Control, and Dynamics*, vol. 46, no. 5, pp. 815–837, May 2023. DOI: 10.2514/1.g007077.

[16] A. Iannelli, D. Gkouletsos, and R. S. Smith, "Robust control design for flexible guidance of the aerodynamic descent of reusable launchers," in *AIAA SCITECH 2023 Forum*, American Institute of Aeronautics and Astronautics, Jan. 2023. DOI: 10.2514/6.2023-2171.

[17] A. De Oliveira and M. Lavagna, "Reusable launchers re-entry controlled dynamics simulator," Proceedings of the 9th European Conference for Aeronautics and Aerospace Sciences. Lille, France, 27th June - 1st July 2022, 2022. DOI: 10.13009/EUCASS2022-6193.

[18] A. De Oliveira and M. Lavagna, "Assessment of reusable launch vehicles re-entry dynamics control effectiveness with enhanced aerodynamics modelling," Proceedings of the 73rd International Astronautical Congress (IAC), Paris, France, 18th - 22nd September 2022, 2022.

[19] P. Simplício, A. Marcos, and S. Bennani, "Reusable launchers: Development of a coupled flight mechanics, guidance, and control benchmark," *Journal of Spacecraft and Rockets*, vol. 57, no. 1, pp. 74–89, Jan. 2020. DOI: 10.2514/1.a34429.

[20] M. Szmuk, T. P. Reynolds, and B. Açıkmeşe, "Successive convexification for real-time six-degree-of-freedom powered descent guidance with state-triggered constraints," *Journal of Guidance, Control, and Dynamics*, vol. 43, no. 8, pp. 1399–1413, Aug. 2020. DOI: 10.2514/1.g004549.

[21] R. C. Nelson, *Flight Stability and Automatic Control*. McGraw-Hill Education, 1989, ISBN: 0070462186.